Novel Transformer with Variable Leakage and Magnetizing Inductances

Angshuman Sharma, Jonathan W. Kimball
Department of Electrical and Computer Engineering
Missouri University of Science and Technology
Rolla, MO, USA
E-mail: asc4v@mst.edu, kimballjw@mst.edu

***Abstract*— This paper introduces the concept of a novel variable inductance transformer (VIT) whose leakage and magnetizing inductances can be varied dynamically and independently to aid the advancement of research in isolated power electronic converters. In this transformer, the leakage inductance can be varied by varying the length of overlap between the primary and secondary windings, while the magnetizing inductance can be varied by varying the air gap between the core legs. Individual controls for the two inductances ensure that one can be varied independent of the other, as needed to satisfy different power conversion objectives. In this paper, the analytical models of the variable leakage and magnetizing inductances are presented. Analytical results are compared with those obtained from Finite Element Method (FEM) and an experimental prototype of a VIT. Analytical solutions of the variable leakage inductance present an error of less than 2.35 % when compared to FEM solutions, while the analytical solutions of the variable magnetizing inductance present a maximum error of 1.82 % when compared to experimental measurements.**

Keywords—image method, leakage inductance, magnetizing inductance, shell-type transformer, variable inductance transformer

I. Introduction

Last decade saw an increasing interest among power electronic researchers in resonant dc-dc converters with integrated magnetics due to their excellent efficiencies at medium and heavy load conditions, fewer passive component count and high power-density capabilities [1], [2]. Yet, only few research has been pursued to understand the effects of change in the value of leakage inductance as the frequency is swept across the operating range of a frequency-controlled converter, or to investigate the effects of inductance ratio (magnetizing inductance /leakage inductance) on the voltage gain and efficiency of the converter at various loads and other operating conditions. These existing knowledge gaps are largely due to the static nature of transformers that characterizes a constant leakage and magnetizing inductance at any given frequency.

This paper introduces the concept of a novel variable inductance transformer (VIT) whose leakage and magnetizing inductances can be varied dynamically and independently across wide user-defined ranges. Fig. 1 shows the concept of a shell-type VIT that is constructed with two ungapped E-shaped ferrite cores. The primary and secondary windings of the VIT are wound around two custom-made bobbins that have a height significantly smaller than the height of the winding window ($h < H$). The leakage inductance of the VIT can be varied by varying the extent of overlap g between the two bobbins. The magnetizing inductance of the VIT can be varied by varying the length of air gap G between the two E cores, which in turn changes the reluctance of the magnetic flux path. By using separate controls for g and G, the two inductances can be varied independently.

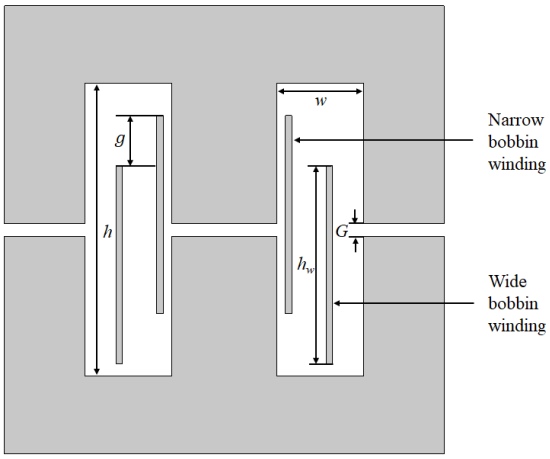

Fig. 1. Variable Inductance Transformer (VIT).

In this paper, analytical models of the variable leakage and magnetizing inductances of the VIT are presented. A 3D Finite Element Method (FEM) model of the VIT is designed and its leakage inductance is evaluated for various overlaps. Further, an experimental prototype of a unity turns ratio VIT is constructed with solid round conductors and its leakage and magnetizing inductances are measured for various overlaps and airgaps, respectively. Finally, the analytical, FEM and experimental results are analyzed and compared for validation of the work.

II. Analytical Modelling of the VIT

A. Variable Leakage Inductance Model

Leakage inductance of a transformer can be calculated from the leakage energy stored inside and outside its volume when perfectly opposed magnetomotive forces (MMFs) are applied to the two windings [3], i.e., $N_1 I_1 = N_2 I_2$, where N_1 and N_2 are the number of primary and secondary turns, and I_1 and I_2 are the primary and secondary currents, respectively. Hence, calculation of leakage inductance is inherently a three-

This material is based upon work supported by the Department of Energy Vehicle Technologies Office under Award Number DE-EE0008449.

dimensional (3D) problem. FEM can calculate the leakage inductance very accurately, but at the expense of high computational effort, especially for 3D FEM [3], [4]. For multi-objective optimization-based designs of isolated converters, analytical leakage inductance models having a lower computational effort with no significant loss in accuracy are preferred [5], [6].

Several analytical and semi-analytical models can be found in the literature that scale the leakage inductance per unit length evaluated across a single 2D plane inside the winding window (Single-2D model) using the mean length turn (MLT) of the windings to obtain the total leakage inductance of the transformer [6]–[13]. Most of these models are based on the magnetic image method, which considers the core as a reflective medium for any current-carrying conductor placed near it. More details about the magnetic image method can be found in [14].

A double-2D model was introduced recently [3], [15], where the leakage inductance per unit length is evaluated across two planes—the inside window (IW) plane and the outside window (OW) plane—hence the name "Double-2D". Total leakage inductance is obtained by adding the product of the two leakage inductances per unit length and their respective partial winding lengths, called leakage lengths. Partial leakage lengths essentially act as scaling factors for the leakage inductances per unit length. Hence, the accuracy of the model depends on the accurate evaluation of the two leakage inductances per unit length and the two partial leakage lengths. Double-2D models are very promising because they can accurately calculate the leakage inductance even when the winding height is significantly smaller than the window height. Fig. 2 illustrates the concept of the Double-2D model, where the IW and OW planes are marked using blue lines. A transition (TR) region is identified between an IW and an OW region, which is crucial for the accurate estimation of the partial leakage lengths.

The general form of the Double-2D model can be written as,

$$L_{lk,\text{Double-2D}} = s_c\left(L'_{2D(\text{IW})}d_{l(\text{IW})} + L'_{2D(\text{OW})}d_{l(\text{OW})}\right) \quad (1)$$

$$s_c = \begin{cases} 1, \text{ core-type transformer} \\ 2, \text{ shell-type transformer} \end{cases}$$

where, $L'_{2D(\text{IW})}$ and $L'_{2D(\text{OW})}$ are the leakage inductances per unit length across the IW and OW planes, and $d_{l(\text{IW})}$ and $d_{l(\text{OW})}$ are the partial leakage lengths for the IW and OW regions, respectively. Methods to calculate these leakage inductances per unit length and partial leakage lengths are discussed below.

1) Calculation of leakage inductances per unit length

The two basic shapes of conductors used for winding transformers are round conductors and rectangular foils. The equations for calculating the field intensities for these two conductor shapes can be found in [3]. Round or Litz wire conductors can be approximated as square conductors of equal cross-sectional area to simplify the formulations in the Cartesian coordinate system [16]. The calculation of leakage inductances per unit length begins with the determination of the exact locations of all conductors in the IW and OW planes. To achieve a variable leakage inductance, g should be varied by moving

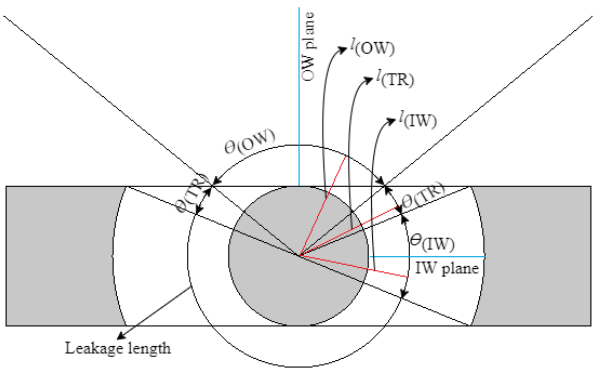

Fig. 2. Double-2D model.

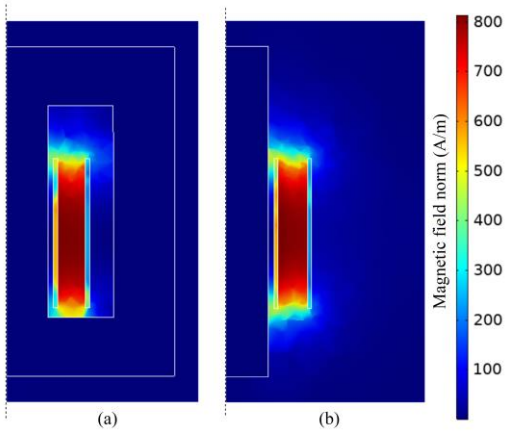

Fig. 3. Magnetic field intensities obtained from the 3D FEM model at $g = 0$ mm: (a) IW plane, and (b) OW plane.

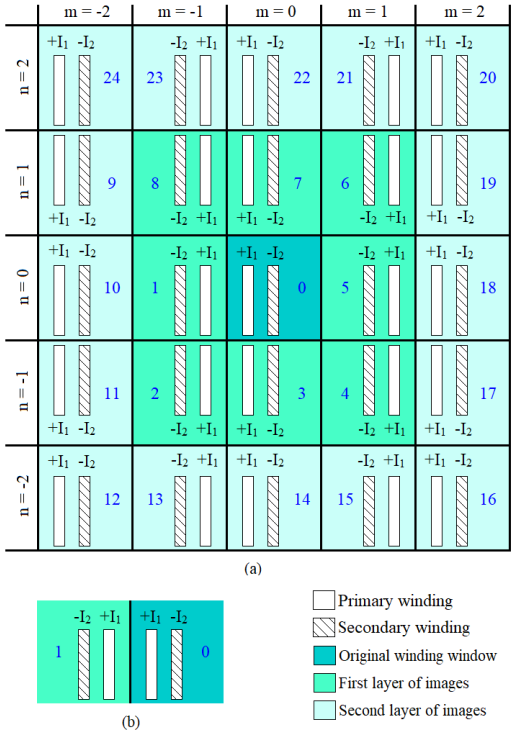

Fig. 4. Image windows resulting from the magnetic image method: (a) IW plane, (b) OW plane.

one of the two bobbins vertically along the central core leg, as indicated in Fig. 1. As such, the y-coordinates of all conductors in the movable bobbin should include g as a variable.

The IW plane is bounded by the core on four sides, as shown in Fig. 3 (a). These four sides act as two pairs of reflective media (mirrors) for a single conductor located in this plane, thereby resulting in an infinite number of image conductors in both x and y directions, as illustrated in Fig. 4 (a). The locations of these image conductors can be determined using [3]. Therefore, at any point $P(x,y)$ in the IW plane, the total field intensity $\vec{H}_P^k$ in k direction due to a single conductor and its images is,

$$\vec{H}_P^k(x,y) = \sum_{j=-n}^{+n}\sum_{i=-m}^{+m}\vec{H}_{P(i,j)}^k(x,y) \tag{2}$$

where, $m \to \infty$, $n \to \infty$, $\vec{H}_{P(i,j)}$ is the field intensity at $P(x,y)$ due to a conductor in the $(i,j)^{\text{th}}$ window, $i = j = 0$ represents the original window, and k represents either x or y direction.

The OW plane, on the other hand, is bounded by the reflective core on one side only, as shown in Fig. 3 (b). As such, a single conductor located in this plane yields one image conductor only, as illustrated in Fig. 4 (b). Therefore, at any point $Q(x,y)$ in the OW plane, the field intensity $\vec{H}_Q^k$ in k direction due to a single conductor and its image is,

$$\vec{H}_Q^k(x,y) = \vec{H}_{Q(\text{original})}^k(x,y) + \vec{H}_{Q(\text{image})}^k(x,y) \tag{3}$$

The total field intensities across the IW and OW planes due to all conductors and their respective images is,

$$\vec{H}_{P(\text{all})}^k(x,y) = \sum_{\text{all}}\vec{H}_P^k(x,y) \tag{4}$$

$$\vec{H}_{Q(\text{all})}^k(x,y) = \sum_{\text{all}}\vec{H}_Q^k(x,y) \tag{5}$$

$$H_{P(\text{all})}^2(x,y) = \left(\vec{H}_{P(\text{all})}^{k=x}(x,y)\right)^2 + \left(\vec{H}_{P(\text{all})}^{k=y}(x,y)\right)^2 \tag{6}$$

$$H_{Q(\text{all})}^2(x,y) = \left(\vec{H}_{Q(\text{all})}^{k=x}(x,y)\right)^2 + \left(\vec{H}_{Q(\text{all})}^{k=y}(x,y)\right)^2 \tag{7}$$

By setting perfectly opposed MMFs in the two windings, the leakage energies per unit length can be calculated using,

$$E'_{2\text{D(IW)}} = \frac{1}{2}\mu_0\int_0^h\int_0^w H_{P(\text{all})}^2(x,y)\,dxdy \tag{8}$$

$$E'_{2\text{D(OW)}} = \frac{1}{2}\mu_0\int_{-\infty}^{\infty}\int_0^{\infty} H_{Q(\text{all})}^2(x,y)\,dxdy \tag{9}$$

where, w and h are the width and height of the winding window.

If I is the primary current, then the leakage inductance per unit length across the IW and OW planes can be finally calculated using,

$$L'_{2\text{D(IW)}} = \frac{2E'_{2\text{D(IW)}}}{I^2} \tag{10}$$

$$L'_{2\text{D(OW)}} = \frac{2E'_{2\text{D(OW)}}}{I^2} \tag{11}$$

2) Calculation of partial leakage lengths

A partial leakage length is a function of the magnetic energy distribution across a plane [15]. First, the energy-weighted mean lengths are calculated for the IW and OW planes using,

$$l_{(\text{IW})} = r_c + \frac{\int_0^h\int_0^w x.H_{P(\text{all})}^2(x,y)dxdy}{\int_0^h\int_0^w H_{P(\text{all})}^2(x,y)dxdy} \tag{12}$$

$$l_{(\text{OW})} = r_c + \frac{\int_{-\infty}^{\infty}\int_0^{\infty} x.H_{Q(\text{all})}^2(x,y)dxdy}{\int_{-\infty}^{\infty}\int_0^{\infty} H_{Q(\text{all})}^2(x,y)dxdy} \tag{13}$$

where, r_c is the radius of the circular central core leg around which concentric windings are wound.

For a circular core leg wound with concentric windings, the partial leakage lengths are also circular. With respect to Fig. 2, the angles subtended at the center of the central core leg (EC-type core) by the IW, TR and OW regions are,

$$\theta_{(\text{IW})} = 2\sin^{-1}\left(\frac{r_c}{w+r_c}\right) \tag{14}$$

$$\theta_{(\text{TR})} = \sin^{-1}\left(\frac{2r_c}{l_{(\text{IW})}+l_{(\text{OW})}}\right) - \frac{\theta_{(\text{IW})}}{2} \tag{15}$$

$$\theta_{(\text{OW})} = \frac{2\pi - s_c\left(\theta_{(\text{IW})}+2\theta_{(\text{TR})}\right)}{s_c} \tag{16}$$

In this work, the TR region is equally divided between an IW and an OW region. Therefore, the angles subtended at the center of the central core leg by the IW and OW regions of the Double-2D model are,

$$\alpha_{(\text{IW})} = \theta_{(\text{IW})} + \theta_{(\text{TR})} \tag{17}$$

$$\alpha_{(\text{OW})} = \theta_{(\text{OW})} + \theta_{(\text{TR})} \tag{18}$$

The angles $\alpha_{(\text{IW})}$ and $\alpha_{(\text{OW})}$ are calculated intuitively in [13], [15]. Finally, the energy-weighted partial leakage lengths can be calculated for the IW and OW regions using,

$$d_{l(\text{IW})} = l_{(\text{IW})}\alpha_{(\text{IW})} \tag{19}$$

$$d_{l(\text{OW})} = l_{(\text{OW})}\alpha_{(\text{OW})} \tag{20}$$

B. Variable Magnetizing Inductance Model

The variable magnetizing inductance of the VIT is calculated by solving its magnetic equivalent circuit for various airgaps G. Fig. 5 represents the magnetic equivalent circuit of the VIT. $\mathcal{R}_c$ represents the reluctance of the core across various segments and $\mathcal{R}_g$ represents the reluctance of each air gap. If L is the length of the core, A_{core} is the cross-sectional area, μ_r is the relative permeability of the core, and μ_0 is the permeability of free space, then the reluctance of the core can be calculated using,

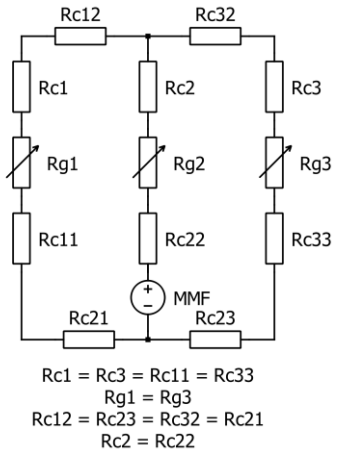

Fig. 5. Magnetic equivalent circuit.

$$\mathcal{R}_c = \frac{L}{\mu_r \mu_0 A_{\text{core}}} \tag{21}$$

The fringing magnetic flux around each air gap must be considered for accurate results. If A_{gap} is the cross-sectional area of the air gap, then the fringing flux factor can be calculated using [17],

$$F = 1 + \frac{G}{\sqrt{A_{\text{gap}}}} ln\left(\frac{2L}{G}\right) \tag{22}$$

The reluctance of the air gap considering fringing flux is,

$$\mathcal{R}_g = \frac{G}{\mu_0 F A_{\text{gap}}} \tag{23}$$

$\mathcal{R}_c$ and $\mathcal{R}_g$ must be calculated for each segment of the flux path. Finally, the total reluctance $\mathcal{R}$ of the flux path is,

$$\mathcal{R} = (\mathcal{R}_{c1} + \mathcal{R}_{c11} + \mathcal{R}_{c12} + \mathcal{R}_{c21} + \mathcal{R}_{g1})||(\mathcal{R}_{c2} + \mathcal{R}_{c22} + \mathcal{R}_{g2})||(\mathcal{R}_{c3} + \mathcal{R}_{c33} + \mathcal{R}_{c32} + \mathcal{R}_{c23} + \mathcal{R}_{g3}) \tag{24}$$

If N_1 is the number of primary turns, then the magnetizing inductance can be calculated for any G using,

$$L_m = N_1^2/\mathcal{R} \tag{25}$$

III. Results

Design specifications of the VIT assumed for this work are presented in Table I. The height of the bobbins is significantly lower than the height of the window (= 44.6 mm for EC 70 core) to ensure that there is enough room for moving one of the bobbins vertically along the core leg. Only single layer windings are considered to demonstrate the concept of VIT, but non-interleaved multilayer windings can also be used.

A. Analytical Model

The Double-2D model used for obtaining the analytical solutions of the variable leakage inductance is simplified by assuming a layer of round conductors as a single rectangular foil having a width equal to $\frac{d\sqrt{\pi}}{2}$ [16], where d is the diameter of the round conductor specified in Table I. From (1), it can be inferred that the accuracy of the Double-2D model depends on the accurate evaluation of the two leakage inductances per unit length as well as the two partial leakage lengths. At $g = 0$ mm, the VIT represents a conventional transformer having a complete overlap between the primary and secondary windings. The leakage inductances per unit length and the partial leakage lengths are evaluated for the conventional transformer case and presented in Table II for validation of the model. All analytical results are obtained using MATLAB R2019a. The leakage inductance per unit length across the IW plane is evaluated by considering the 24 nearest images to the original window, i.e. the two full layers of images shown in Fig. 4 (a).

TABLE I
Design Specifications

Description	Value
Core type and size (part)	EC 70 (EPCOS B66343)
Height of the bobbins	31.5 mm
External diameter of narrow bobbin	19 mm
External diameter of wide bobbin	32.5 mm
Thickness of the bobbins	1.5 mm
Turns ratio	1:1
Number of turns	26
Number of layers	1
Primary current	1 A
Conductor shape/AWG/diameter	Round/19/0.912 mm
Test frequency	1 kHz
Relative permeability of the core	1360
Range of g	0 – 10 mm
Range of G	0.1 – 5 mm

B. FEM Model

A 3D FEM model of the VIT is designed in COMSOL Multiphysics 5.5 to investigate the accuracy of the Double-2D model. The FEM model is wound with rectangular foils that have a width equal to $\frac{d\sqrt{\pi}}{2}$, as stated above. Figs. 3 and 6 plot the magnetic field intensities across the IW and OW planes at $g = 0$ mm and $g = 10$ mm, respectively. It is evident from these two figures that the field intensities in Fig. 6 is much higher than those in Fig. 3.

The partial leakage lengths are not readily available from the FEM model. To investigate the accuracy of the analytically calculated partial leakage lengths, a horizontal cut line is plotted along the width of each plane that always passes through the center of the overlapped winding. The energy-weighted mean lengths are then calculated using,

$$l_{(\text{IW})} = r_c + \frac{\int_0^W x.H^2(x)dx}{\int_0^W H^2(x)dx} \tag{26}$$

$$l_{(\text{OW})} = r_c + \frac{\int_0^\infty x.H^2(x)dx}{\int_0^\infty H^2(x)dx} \tag{27}$$

The angles subtended at the center of the central core leg by the IW and OW regions, and consequently the partial leakage

TABLE II
LEAKAGE INDUCTANCE AT $g = 0$ MM

Category of results		$L'_{2D(IW)}$ (uH/m)	$L'_{2D(OW)}$ (uH/m)	$d_{l(IW)}$ (mm)	$d_{l(ow)}$ (mm)	L_{lk} (μH)	Error (%)
Analytical		153.27	152.54	14.266	27.494	12.761	0.2
3D FEM	Actual	155.11	149.26	-	-	12.736	0
	Calculated leakage lengths			14.213	27.148	12.514	– 1.74

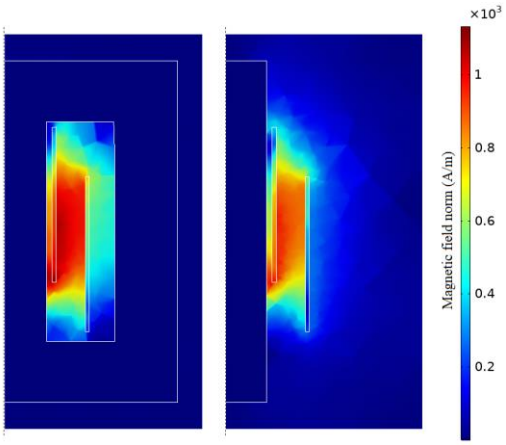

Fig. 6. Magnetic field intensities obtained from the 3D FEM model at $g = 10$ mm: (a) IW plane, and (b) OW plane.

lengths are calculated using (14) – (20) for various overlaps. The results obtained from the 3D FEM model are considered as standards for comparing the model errors presented in Table II. The variable magnetizing inductance of the VIT is not modelled in FEM because the analytically calculated values of the magnetizing inductance are in full agreement with the experimentally measured values.

C. Experimental Model

An experimental model of the VIT is deigned according to specifications and is depicted in Fig. 7. Two ungapped E-shaped ferrite cores are used to build the shell-type transformer. Perfect round conductors are used to construct the transformer windings. Although either bobbin may be used as the movable one to vary g, this specific work uses the narrow bobbin as the movable one for mechanical reasons. A single linear actuator is used to move the narrow bobbin vertically along the central core leg, while two identical linear actuators are used to move the upper E core vertically in order to vary G. Speed of the linear actuators can be controlled using the operating voltage. According to specifications, the linear actuators exhibit a speed of approximately 15 mm/second at 12 V. In this work, the linear actuators are operated at 4 V to achieve a speed of 5 mm/second. Using a microcontroller, the linear actuators can be operated for definite time intervals to achieve the desired g and G. An LCR meter is used to measure the leakage and magnetizing inductances of the experimental model at 1 kHz test frequency. A high precision digital gauge, having a resolution of 0.01 mm, is used for measuring g and G.

D. Variable Leakage Inductance

Fig. 8 plots the variation of analytically calculated, FEM simulated, and experimentally measured values of the leakage inductance with g. From Table II, it is evident that the Double-

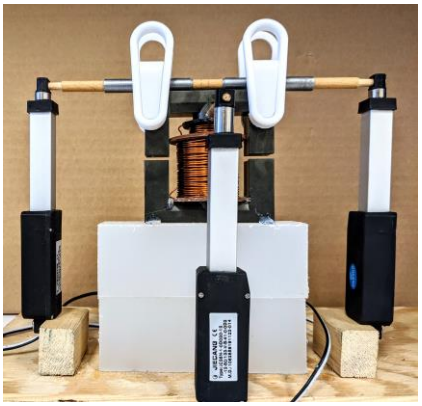

Fig. 7. Experimental prototype of the VIT.

2D model is fairly accurate for calculating the leakage inductance of a conventional transformer where $g = 0$ mm. But the same may not be inferred for $g > 0$ mm, as indicated by the black curve in Fig. 8, which shows that the error between the analytically evaluated and FEM simulated values of the leakage inductance increases with g. The main reason for this error is that the image method-based Double-2D model is an ideal model that neglects the fringing flux across the edges of a conductor. In order to limit the error at $g > 0$ mm, a correction factor k_t is introduced in this paper, where

$$k_t = \sqrt{1 + {}^{g}/_{h}} \tag{28}$$

Therefore, the corrected leakage inductance of the VIT can be analytically calculated using,

$$L_{lk,\text{VIT}} = k_t \times L_{lk,\text{Double-2D}} \tag{29}$$

The correction factor could reduce the error significantly below 2.35 % (observed at $g = 4$ mm), as indicated by the blue curve in Fig. 8. As g goes from 0 to 10 mm, the leakage inductance of the experimental model increases from 13.2 μH to 23.8 μH. The FEM simulated values of the leakage inductance closely follow the experimentally measured values and a maximum error of 3.64 % can be observed at $g = 0$ mm.

E. Variable Magnetizing Inductance

Fig. 9 plots the variation of analytically calculated and experimentally measured values of the magnetizing inductance with G. As G is increased from 0.1 to 5 mm, the reluctance of the flux path increases and the magnetizing inductance of the experimental model drops from 868.5 μH to 61 μH. The analytically calculated magnetizing inductance closely follow the experimentally measured values with a maximum error of 1.82 % observed at $G = 0.75$ mm.

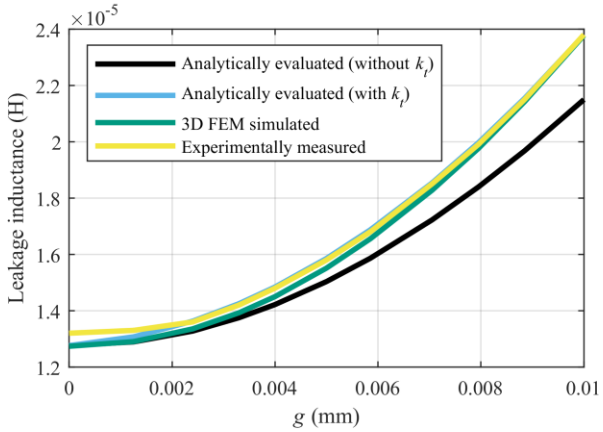

Fig. 8. Plot showing the variation of leakage inductance with g.

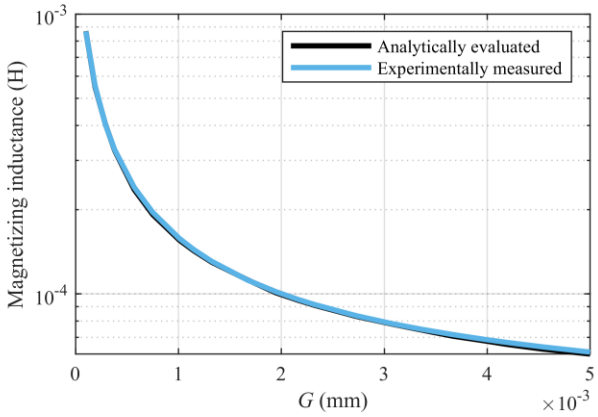

Fig. 9. Plot showing the variation of magnetizing inductance with G.

Since the extent of overlap between the two bobbins is independent of the reluctance of the flux path, a variation in leakage inductance does not affect the magnetizing inductance. However, a small variation may be observed in the leakage inductance as the airgap is varied. This is because a change in airgap changes the areas of the IW and OW planes under investigation. Nevertheless, the range of overlap is too small to cause any significant effect on the leakage inductance. Thus, the leakage inductance and the magnetizing inductance of the VIT can be controlled independently.

IV. Conclusion

The key contributions of this paper are: a) introduction to the concept of variable inductance transformer, b) analytical modelling of the variable leakage and magnetizing inductances, c) design of an experimental prototype, and d) validation of the analytical models using 3D FEM simulations and experimental measurements. The leakage inductance of the experimental model increased from 13.2 µH to 23.8 µH as the extent of overlap between the two windings was reduced by 10 mm. Again, the magnetizing inductance of the experimental model dropped from 868.5 µH to 61 µH as the airgap between the core legs was increased by 4.9 mm. The two inductances were controlled independently and dynamically across their specified ranges using linear actuators. The analytical model of the variable leakage inductance exhibited a maximum error of 2.35 %, while that of the variable magnetizing inductance showed a maximum error of 1.82 %. The proposed concept of the VIT can also be extended to other transformer core geometries and non-interleaved multilayer windings. VIT can prove to be a beneficial tool for the advancement of research in resonant converters.

References

[1] J. H. Jung, H. S. Kim, M. H. Ryu, and J. W. Baek, "Design methodology of bidirectional CLLC resonant converter for high-frequency isolation of DC distribution systems," IEEE Transactions on Power Electronics, vol. 28, no. 4, pp. 1741–1755, 2013.

[2] X. Fang, H. Hu, Z. J. Shen, and I. Batarseh, "Operation mode analysis and peak gain approximation of the LLC resonant converter," *IEEE Transactions on Power Electronics*, vol. 27, no. 4, pp. 1985–1995, 2012.

[3] A. Fouineau, M. A. Raulet, B. Lefebvre, N. Burais, and F. Sixdenier, "Semi-analytical methods for calculation of leakage inductance and frequency-dependent resistance of windings in transformers," *IEEE Transactions on Magnetics*, vol. 54, no. 10, pp. 1–10, 2018.

[4] M. Nazmunnahar, S. Simizu, P. R. Ohodnicki, S. Bhattacharya, and M. E. McHenry, "Finite-element analysis modeling of high-frequency single-phase transformers enabled by metal amorphous nanocomposites and calculation of leakage inductance for different winding topologies," *IEEE Transactions on Magnetics*, vol. 55, no. 7, 2019.

[5] A. Garcia-Bediaga, I. Villar, A. Rujas, L. Mir, and A. Rufer, "Multiobjective optimization of medium-frequency transformers for isolated soft-switching converters using a genetic algorithm," *IEEE Transactions on Power Electronics*, vol. 32, no. 4, pp. 2995–3006, 2017.

[6] R. Schlesinger and J. Biela, "Comparison of analytical models of transformer leakage inductance: accuracy versus computational effort," *IEEE Transactions on Power Electronics*, vol. 36, no. 1, pp. 146–156, 2021.

[7] A. K. Das, Z. Wei, S. Cao, S. Vaisambhayana, H. Tian, A. Tripathi, and P. C. Kjær, "Accurate calculation of leakage inductance for balanced and fractional-interleaved winding in medium-frequency high-power transformer," in *Proceedings - 2017 IEEE Southern Power Electronics Conference, SPEC 2017*, Peurto Varas, Chile, 2017, pp. 1–6.

[8] Z. Ouyang, O. C. Thomsen, and M. A. E. Andersen, "The analysis and comparison of leakage inductance in different winding arrangements for planar transformer," in *2009 International Conference on Power Electronics and Drive Systems (PEDS)*, Taipei, Taiwan, 2009, pp. 1143–1148.

[9] P. Gómez and F. de León, "Accurate and efficient computation of the inductance matrix of transformer windings for the simulation of very fast transients," *IEEE Transactions on Power Delivery*, vol. 26, no. 3, pp. 1423–1431, 2011.

[10] M. Eslamian and B. Vahidi, "New methods for computation of the inductance matrix of transformer windings for very fast transients studies," *IEEE Transactions on Power Delivery*, vol. 27, no. 4, pp. 2326–2333, 2012

[11] M. Lambert, F. Sirois, M. Martinez-Duro, and J. Mahseredjian, "Analytical calculation of leakage inductance for low-frequency transformer modeling," *IEEE Transactions on Power Delivery*, vol. 28, no. 1, pp. 507–515, 2013.

[12] X. Margueron, J. P. Keradec, and D. Magot, "Analytical calculation of static leakage inductances of HF transformers using PEEC formulas," *IEEE Transactions on Industry Applications*, vol. 43, no. 4, pp. 884–892, 2007.

[13] A. F. Hoke and C. R. Sullivan, "An improved two-dimensional numerical modeling method for E-core transformers," in *Conference Proceedings - IEEE Applied Power Electronics Conference and Exposition - APEC*, Dallas, TX, 2002, pp. 151–157.

[14] P. Hammond, "Electric and magnetic images," in *Proceedings of the IEE-Part C: Monographs*, 1960, vol. 107, no. 12, pp. 306–313.

[15] R. Schlesinger and J. Biela, "Leakage inductance modelling of transformers: accurate and fast models to scale the leakage inductance per unit length," in *2020 22nd European Conference on Power Electronics*

and Applications, EPE 2020 ECCE Europe, Lyon, France, 2020, pp. 1–11.

[16] M. Mogorovic and D. Dujic, "Medium frequency transformer leakage inductance modeling and experimental verification," in *2017 IEEE Energy Conversion Congress and Exposition, ECCE 2017*, Cincinnati, OH, 2017, pp. 419–424.

[17] Stan Zurek, "Flux fringing," *Encyclopedia Magnetica*, 2012. https://www.e-magnetica.pl/doku.php/flux_fringing (accessed Nov. 03, 2020).